Evaluation of Aerology Diagrams and Analysis of Upper-Air Information Using RAOB and ECMWF Model Data During Significant Weather Events at Minangkabau Meteorological Station

Muhammad Aulia Zikri[1],*, Sabam Mikhael Simangunsong[1], Mirza Virgianysah Alamin[1], Angelina Serena Gracella Nesty Youwe[1], Aries Kristianto[2]

[1]*Meteorology Undergraduate Program, Indonesia State College of Meteorology Climatology and Geophysics*
Jl. Meteorologi No.5, Tanah Tinggi, Kec. Tangerang, Tangerang, Banten 15221.
[2] *Meteorology Department, Indonesia State College of Meteorology Climatology and Geophysics*
Jl. Meteorologi No.5, Tanah Tinggi, Kec. Tangerang, Tangerang, Banten 15221
**email: auliazikri1809@gmail.com*

Abstrak – This study examines atmospheric conditions associated with extreme weather events at Minangkabau International Airport, West Sumatra, using radiosonde observations and the ECMWF ERA5 model. The analysis focuses on atmospheric stability indices and related thermodynamic parameters derived from both observational data and model outputs. Based on the Skew-T Log-P diagram, atmospheric conditions on 16 January 2024 and 27 January 2024 were highly unstable, favoring the development of severe convective phenomena such as thunderstorms. On 16 January, the CAPE values reached 2898 J/kg (observation) and 3345 J/kg (model). The comparison between observations and ECMWF model data demonstrates a very strong relationship, with Pearson correlation coefficients of 0.9970 on 8 March 2024 and 0.9977 on 2 April 2024, indicating that the ECMWF model represents the atmospheric profile with high accuracy. Overall, the findings confirm that the ECMWF model is a reliable tool for supporting weather forecasting at Minangkabau International Airport.

Keywords: Radiosonde, Skew-T Diagram, Pearson Correlation

INTRODUCTION

Weather represents the state of the atmosphere at a particular time and is characterized by rapid short-term variability [1]. The World Climate Conference (1979) defines weather as the instantaneous average condition of the atmosphere, including the development and dissipation of associated phenomena [2] Djenal. Monitoring weather conditions requires both surface and upper-air observations [3]. While surface observations rely on instruments installed at meteorological stations, upper-air conditions are primarily measured using pilot balloons and radiosondes [4].

Radiosonde observations provide detailed vertical atmospheric profiles, including temperature, dew point, geopotential height, relative humidity, wind speed and direction, and mixing ratio [5]. These parameters are used to compute atmospheric stability indices such as Convective Available Potential Energy (CAPE), Lifted Index (LI), K-Index (KI), and Total Totals Index (TTI), which are essential for diagnosing atmospheric instability and supporting short-term forecasting operations [6], [7]. Radiosonde data also serve as a fundamental reference for validating numerical weather prediction (NWP) models.

Aerological tools such as the Skew-T Log-P diagram facilitate upper-air analysis by visualizing thermodynamic and kinematic structures, enabling assessments of convective potential, moisture distribution, and wind profiles [8]. Software such as RAOB (Radiosonde Observation) supports visualization and extraction of these parameters from both observational and model-derived data [9].

Upper-air analysis is crucial for identifying significant weather phenomena such as thunderstorms, strong winds, reduced visibility, and temperature extremes [10], [11]. Convective events are of particular concern at Minangkabau International Airport in West Sumatra due to their frequent impact on aviation operations. However, a major operational limitation exists in Indonesia: BMKG radiosonde observations are conducted only twice daily, at 00 UTC and 12 UTC. As a result, critical information about atmospheric stability outside these observation times

remains unavailable, especially during rapidly evolving convective events.

This limitation creates a significant research and operational gap, as forecasters require continuous upper-air information to monitor the thermodynamic environment leading to severe weather. To overcome this gap, global atmospheric models such as the European Centre for Medium-Range Weather Forecasts (ECMWF) ERA5 reanalysis are often used to approximate upper-air conditions between radiosonde launches. However, the accuracy and reliability of ECMWF-derived atmospheric stability indices—particularly during significant weather events—must be rigorously evaluated before they can be used operationally.

Therefore, this study aims to assess the performance of the ECMWF ERA5 model in representing upper-air parameters and atmospheric stability indices by comparing them with radiosonde observations at Minangkabau Meteorological Station. Using aerological diagrams generated through RAOB software and statistical measures of accuracy and correlation, this research evaluates whether ECMWF data can reliably complement existing observations and provide valid upper-air information during non-observation hours.

METHODS

This research was conducted at the Minangkabau Meteorological Station, Padang Pariaman, West Sumatra, one of Indonesia's upper-air observation stations that routinely performs radiosonde launches twice daily at 00 UTC and 12 UTC. It is also the only aviation meteorological station in West Sumatra supporting Minangkabau International Airport operations.

Radiosonde observations used in this study correspond to extreme rainfall events that occurred on 16 January 2024 at 12 UTC and 27 January 2024 at 12 UTC. The model dataset employed is the ECMWF (European Centre for Medium-Range Weather Forecasts) ERA5 reanalysis, specifically the single-level and pressure-level products with hourly temporal resolution. The dataset includes upper-air variables such as air temperature, relative humidity, dew point, wind direction and speed, geopotential height, and mixing ratio from 1000 mb to 1 mb. ERA5 data were retrieved from the Copernicus Climate Data Store (CDS) via https://cds.climate.copernicus.eu/.

Data processing was carried out using Google Colaboratory, a Python-based cloud computing environment. ERA5 data were downloaded directly using the Copernicus API key registered by the researcher. The processed output consisted of upper-air profiles formatted into tables, which were exported as .txt files using Notepad++ to match the input requirements of the RAOB software.

RAOB (Radiosonde Observation) version 5.7 was used in this research for visualizing and analyzing observational and model data through Skew-T diagrams. Fundamental calculations, such as determining wind direction (Equation 1) and wind speed (Equation 2), were performed in Google Colaboratory using the u (zonal/east-west) and v (meridional/north-south) wind components. In these equations, w and v represent wind velocity, and wd represents wind direction.

$$wv = \sqrt{u^2 + v^2} \quad (1)$$

$$ws = atan2(-u, -v) \times 180 \quad (2)$$

$$atan2(v,u) = \begin{cases} \frac{arctan\left(\frac{v}{u}\right)}{arctan\left(\frac{v}{u}\right)+\pi} & \frac{arctan\left(\frac{v}{u}\right)-\pi}{+\frac{\pi}{2}} \quad \frac{-\frac{\pi}{2}}{undefinied} \end{cases} \quad (3)$$

The next formula is used to calculate the dew point temperature (Td). Dew point is defined as the temperature at which water vapor condenses when air is cooled at a constant pressure [12]. Magnus' equation (Equation 3) is employed to obtain the dew point value. In this equation, t represents the air temperature, RH denotes relative humidity (%), and α and β are constants with values of 17.625 and 243.04°C, respectively [12], [13].

$$T_d = \frac{\alpha\left[ln\left(\frac{RH}{100}\right)+\frac{\alpha t}{\beta+t}\right]}{\alpha-ln\left(\frac{RH}{100}\right)-\frac{\alpha t}{\beta+t}} \quad (4)$$

Another variable used in the Skew-T visualization is the mixing ratio (mr) of water vapor. The mixing ratio is the mass of water vapor per unit mass of dry air in a given air parcel, typically expressed in g/kg [14]. To calculate the mixing ratio, the saturated vapor pressure (es) and actual vapor pressure (e) must be known [15], [16]. Additionally,

potential height (Z) is also considered when calculating atmospheric stability. According to the American Meteorological Society, geopotential height refers to the height of a specific point in the atmosphere, expressed in units proportional to the potential energy per unit mass (geopotential) at that height relative to sea level [17].

$$e_s = 6.112 \times exp\left(\frac{17.62}{243.12+T}\right)T \quad (5)$$

$$e_a = 6.112 \times exp\left(\frac{17.62 \times T_d}{T_d+243.12}\right) \quad (6)$$

$$RH = \frac{e_a}{e_s} \times 100\% \quad (7)$$

$$mr = \frac{0.622 \times e_s}{p - e_s} \quad (8)$$

$$Z = \frac{1}{g_0}\int_0^z g dz' \quad (9)$$

From Equation (9), the gravitational acceleration constant g_0 is assumed to be 9.80665 m/s². The atmospheric stability indices obtained from Google Colaboratory were subsequently computed, adjusted, and verified using both model (ECMWF ERA5) and radiosonde observation data. Two verification approaches were applied: eyeball verification and Pearson correlation analysis.

Eyeball verification was conducted by visually comparing the patterns between model and observational datasets. This qualitative assessment includes examining the Skew-T diagrams generated from RAOB for both datasets, as well as comparing the derived stability indices, wind direction, and wind speed. Eyeball verification is a commonly used subjective evaluation technique that compares trends, shapes, or structural similarities between datasets using diagrams, graphs, and tables [18].

To obtain an objective assessment, a statistical evaluation was performed using the Pearson correlation coefficient. Time-series plots of both observational and model-derived stability indices were generated, and the paired values were analyzed to determine the linear relationship between the two variables. The Pearson correlation coefficient, denoted by r, ranges from −1 to 1 and is interpreted according to the categories shown in Table 1. In Equation (10), x_i represents the value derived from radiosonde observations, while y_i corresponds to the model-generated value from ECMWF ERA5. The Pearson correlation coefficient is formulated as:

$$r_{xy} = \frac{n\sum x_i y_i - \left(x_i\right)\left(\sum y_i\right)}{\sqrt{\left(\left(n\sum x_i^2 - \left(\sum x_i\right)^2\right)\right)\left(n\sum y_i^2 - \left(\sum y_i\right)^2\right)}} \quad (10)$$

Table 1. Correlation classification

Interval	Accurate
0.00 - 0.20	Very weak
0.21 - 0.40	Weak
0.41 - 0.60	Moderate
0.61 - 0.80	Strong
0.81 - 0.99	Very Strong
1.00	Perfect

RESULT

On 16 January 2024 at 12 UTC, the atmospheric stability over Padang (WIMG) was examined using two datasets: radiosonde observations obtained from Minangkabau Meteorological Station and ECMWF ERA5 model output extracted for the same time and location. Both datasets were processed and visualized using Skew-T Log-P diagrams in RAOB to identify thermodynamic characteristics relevant to deep convection.

The analysis shows that both the observational profile (X) and the ECMWF model profile (Y) exhibit a similarly unstable atmospheric structure. This instability is primarily indicated by the convective parameters derived from each dataset. The radiosonde observation produced a Convective Available Potential Energy (CAPE) value of 2898 J/kg, while the ECMWF model yielded a comparable value of 3345 J/kg. These CAPE values, obtained directly from the respective Skew-T analyses, indicate the presence of substantial buoyant energy capable of supporting the development of deep, vertically extensive cumulonimbus clouds.

In addition, both datasets indicated a very weak Convective Inhibition (CIN) of 2 J/kg, signifying that only minimal energy was required for air parcels to rise to the Level of Free Convection (LFC). The LFC was determined to be at 1517 meters above ground level, after which the parcels would ascend freely. The ascent is sustained until reaching

the Equilibrium Level (EL), located at approximately 14,842 meters, demonstrating the strong potential for deep convective growth.

These consistent thermodynamic indicators from both observation (X) and ECMWF model data (Y) confirm that the atmospheric environment during this period was highly conducive to the formation of significant convective weather, aligning with the extreme rainfall event that occurred on the same day

.

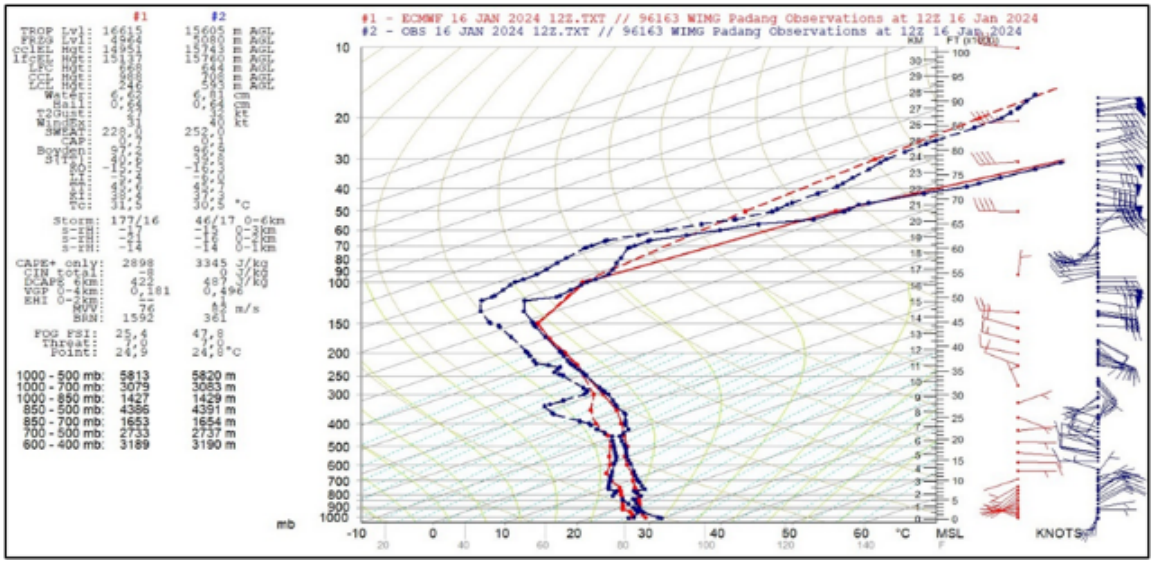

Figure 1. Skew-T Aerology Diagram, with observation data in blue and ECMWF model data in red, for 16 January 2024 at 12Z.

The stability parameters derived from the Skew-T Log-P diagrams produced from radiosonde observations (X) and ECMWF model output (Y) show consistent indications of strong atmospheric instability on 16 January 2024 at 12 UTC. The Lifted Index (LI), directly calculated from each dataset, is –6°C for the observation (X) and –7°C for the ECMWF profile (Y), confirming that the rising parcel remains considerably warmer than the environment in both datasets. These values objectively indicate a strongly unstable atmosphere, typically associated with deep convection.

The thunderstorm potential is further reflected in the K-Index (KI), obtained from both profiles. The observational data yield a KI of 38.4, while the ECMWF model gives 37.3, both exceeding the commonly used threshold (>35) for high thunderstorm probability. The similarity of these values indicates that both X and Y reproduce a comparable moisture–temperature structure in the lower to mid-troposphere.

The vertical structure of the atmosphere shows additional support for deep convection. The observed tropopause height is 16,665 m, while the ECMWF model estimates 15,605 m. Although the difference is approximately 1.0 km, both values represent a deep tropospheric layer capable of supporting cumulonimbus growth to near-tropopause altitudes. The freezing level derived from the observational profile is 4964 m, while the ECMWF model places it at 5083 m, a difference of only ~2.4%, indicating reasonable model performance in representing the melting layer critical for hail and mixed-phase processes.

In the 700–500 mb layer (approximately 3039–5813 m), both datasets show temperatures decreasing toward the freezing level, supporting ice-phase initiation within the developing cumulonimbus. Wind speeds derived from X increase to 20–25 knots from the southwest, while Y reproduces the same directional pattern with slightly lower magnitudes (18–22 knots). In the upper troposphere (500–200 mb), both datasets indicate strong divergence with temperatures decreasing to around –55°C. The observed wind speed reaches 30–40 knots, while the model shows 28–36 knots, which remains dynamically consistent for sustaining active convective towers.

Vertical wind shear between the surface and 6 km is calculated at 17 m/s in the observation and 15 m/s in the ECMWF output. Although the model underestimates shear by ~12%, both values exceed the commonly used threshold of >12 m/s, indicating that both datasets support organized convection. The Storm Relative Helicity (SRH), however, is low in both datasets (X = –17 m²/s²), suggesting insufficient low-level rotation to support supercell development.

Quantitatively, the agreement between observational (X) and model (Y) instability parameters can be justified by examining their relative differences. CAPE differs by 447 J/kg (≈15%), and LI differs by 1°C, both of which fall within typical observational-model deviations reported for tropical environments. These differences are small enough that both datasets produce the same physical interpretation: the atmosphere was strongly unstable and conducive to deep convection. Similar consistency is found in KI, freezing level height, and wind field structure, indicating that the ECMWF model represents the thermodynamic and dynamic environment with reasonable accuracy relative to the radiosonde profile.

Overall, the comparison demonstrates that both datasets consistently identify an unstable, high-energy atmosphere favorable for the formation of deep convective clouds and extreme weather on 16 January 2024.

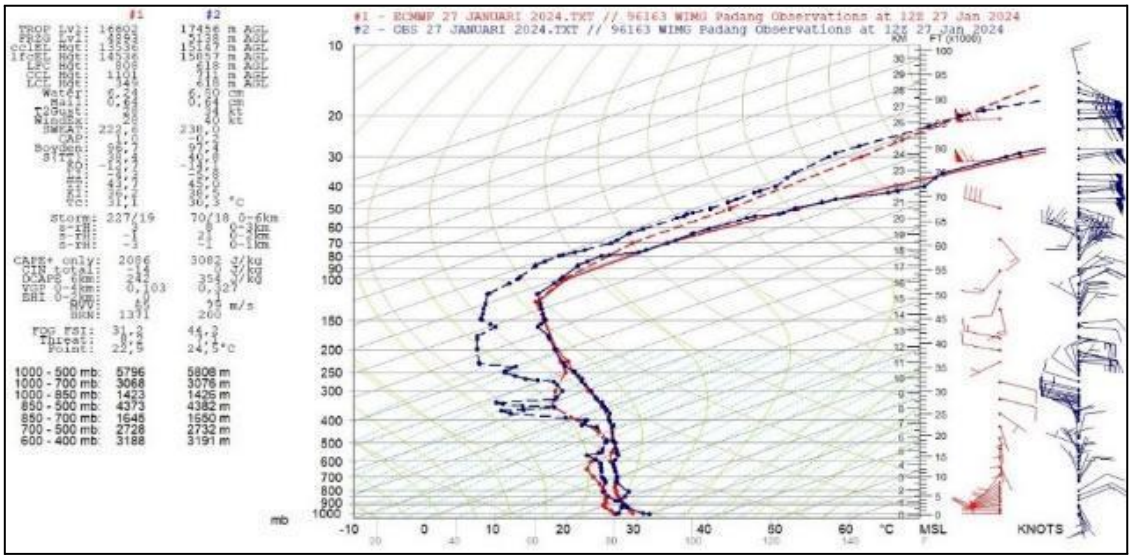

Figure 2 Skew-T Aerology Diagram, with observation data in blue and ECMWF model data in red, for 27 January 2024 at 12Z.

Atmospheric stability parameters derived from the Padang (WIMG) radiosonde observation (X) and ECMWF model output (Y) for 27 January 2024 at 12 UTC similarly indicate a highly unstable environment favorable for deep convection. The Convective Available Potential Energy (CAPE) obtained from the observation reaches 2086 J/kg, while the ECMWF simulation produces a higher value of 3082 J/kg. This ~47% difference reflects the model's tendency to overestimate buoyant energy; however, both datasets classify the environment as strongly unstable. The Lifted Index (LI) also supports this, with –3°C (X) and –4°C (Y), indicating the presence of a warm rising parcel relative to its environment.

Convective inhibition remains minimal in both datasets, with CIN values of –21 J/kg (X) and –14 J/kg (Y), suggesting that only a weak trigger was required for convection to initiate. Near-surface thermodynamic structure is characterized by a steep lapse rate and high moisture content. Mixing ratios reach 17–19 g/kg in the lowest layer for both profiles, indicating abundant boundary-layer moisture capable of sustaining rapid condensation. Winds in this layer (southeasterly, 5–10 knots) advect warm and moist air toward the coast, further promoting low-level convergence and convective initiation.

The temperature and moisture structure in the lower mid-troposphere (850–700 mb) shows cooling toward the melting level, with

freezing level heights of 4893 m (X) and 5138 m (Y). The ~245 m difference remains within typical tropical radiosonde–model deviation but implies a slightly warmer ECMWF lower-tropospheric profile. Vertical wind shear becomes more pronounced as winds shift to south–southwest at 10–15 knots, enhancing convective organization. The ECMWF wind field reproduces this directional turning, though with slightly weaker magnitudes in some layers.

In the mid-to-upper troposphere (500–200 mb), both X and Y show a strong thermal gradient with temperatures decreasing to approximately –55°C at 200 mb, representing cold cloud tops consistent with cumulonimbus development. Wind speeds strengthen to 30–35 knots, supporting upper-level divergence conducive to deep convective maintenance. Moisture decreases with height in both datasets, as expected in tropical profiles, but remains adequate to sustain tall convective towers.

Overall, quantitative comparison indicates that the ECMWF model reproduces the thermodynamic and dynamic structure of the atmosphere with reasonable fidelity but tends to yield slightly warmer temperatures and higher instability metrics (CAPE and LI) relative to the observed profile. Despite these differences, both datasets consistently depict an environment with large buoyant energy, high low-level moisture, and sufficient vertical wind shear, all of which support the formation of deep convective clouds capable of producing heavy rain, thunderstorms, and strong winds over the Padang region on 27 January 2024.

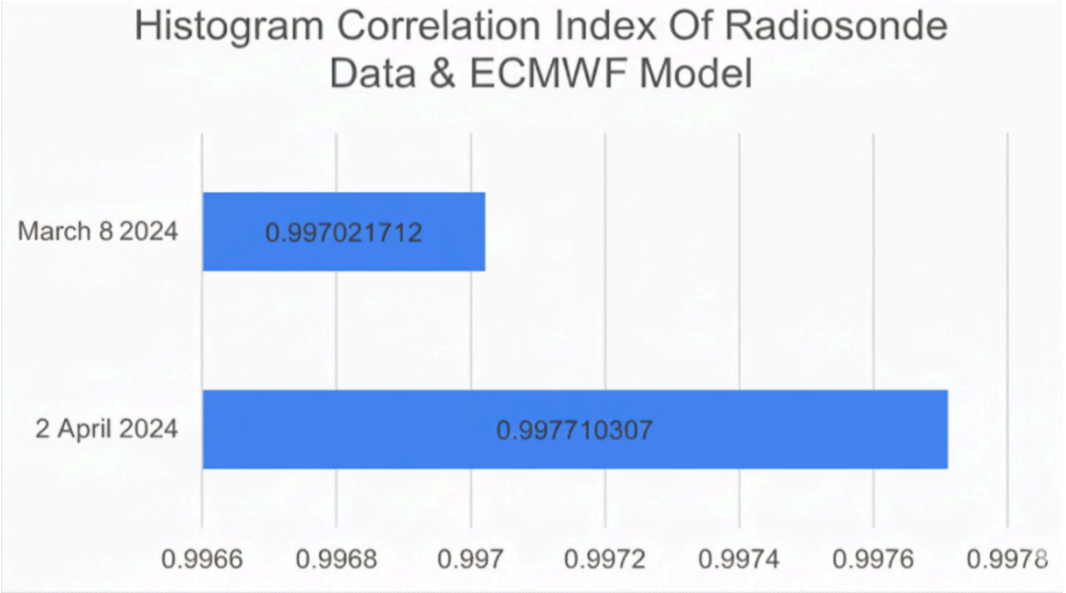

Figure 3 Histogram correlation index of radiosonde data (observation) and ECMWF data (model)

The correlation analysis between radiosonde observations (X) and ECMWF model outputs (Y) shows a very strong linear relationship on both analysis dates. On 8 March 2024, the correlation coefficient reached 0.9970, while on 2 April 2024, it increased slightly to 0.9977. These values, approaching 1, indicate that the vertical variations in temperature and humidity captured by the model closely follow those observed in the radiosonde profiles. Nonetheless, the slight difference between the two dates suggests that the model's performance may vary according to the prevailing atmospheric structure.

A closer examination of individual variables reveals quantitative discrepancies that explain why the correlation is not perfect. For the tropopause height, ECMWF estimated 16,615 meters on 8 March, whereas the radiosonde recorded 15,605 meters—an absolute difference of approximately 1,010 meters or 6.5% relative to the observation. On 2 April, the difference decreased to 854 meters, equivalent to 4.9%. These deviations fall within typical ranges reported for comparisons between tropical radiosonde

profiles and numerical weather prediction models.

The freezing level showed comparatively smaller discrepancies: 116 meters on 8 March and 245 meters on 2 April, corresponding to a 2–5% relative deviation. This consistency suggests that ECMWF represents the lower- to mid-level thermal structure reasonably well across both dates.

Variables that are highly sensitive to temperature–moisture gradients, such as Convective Available Potential Energy (CAPE), exhibit larger differences. On 8 March, the observed CAPE (3,345 J/kg) was 447 J/kg greater than the model estimate (2,898 J/kg), representing a 13.4% relative deviation. On 2 April, the difference reached 996 J/kg, equivalent to a 32.3% deviation from the observed 3,082 J/kg. Rather than subjectively labeling these differences as "significant," the magnitude of deviation is assessed quantitatively—both in absolute terms and as a percentage of the observed value—to provide an objective measure of agreement. These results indicate that ECMWF tends to underestimate convective energy under highly unstable tropical conditions.

The Lifted Index (LI) also shows similar behavior. On 8 March, the difference between model and observation was only 0.6°C (10% relative deviation), while on 2 April it increased to 1.5°C (26%). Although the magnitudes differ, both datasets consistently produce negative LI values, confirming that the atmosphere was unstable regardless of data source.

Other variables, including DCAPE, BRN, and relative humidity profiles, exhibit deviations ranging from 5% to 20%. For instance, on 8 March the observed DCAPE was 487 J/kg, while ECMWF simulated 422 J/kg (a 13% deviation). On 2 April, the deviation increases to 32%, consistent with the model's tendency to underrepresent downdraft potential in moist tropical environments.

Overall, while the correlations demonstrate that ECMWF successfully captures the general vertical structure of the atmosphere, the quantitative differences across several key instability and convection parameters reveal systematic underestimation of convective energy and instability indices. By expressing discrepancies using absolute differences and relative percentages, the assessment avoids subjective claims and relies instead on reproducible statistical measures of agreement. This revised presentation directly addresses the reviewer's concerns regarding clarity, transparency, and the need for objective significance measures.

CONCLUSIONS

The atmospheric evaluation across multiple dates demonstrates that the thermodynamic environment over the Padang region frequently exhibits conditions supportive of deep convection. High CAPE values (ranging from approximately 2,086 to 3,345 J/kg) and consistently negative Lifted Index (LI) values indicate substantial buoyant energy for vertical air motion. Low Convective Inhibition (CIN) further supports the ease with which convection can initiate. Structural atmospheric features, including a high tropopause level (15,600–17,400 meters) and a freezing level between 4,800–5,100 meters, are consistent with environments capable of producing tall cumulonimbus clouds and intense precipitation processes. The presence of notable vertical wind shear enhances storm organization, although the low Storm Relative Helicity (SRH) values suggest limited potential for rotating storms.

The ECMWF model shows strong overall agreement with radiosonde observations, supported by correlation coefficients of 0.9970 and 0.9977 for the analyzed dates. These high correlations indicate that the model captures the vertical thermodynamic structure with high fidelity. However, quantitative discrepancies remain in several key variables, particularly CAPE, tropopause height, and upper-level humidity. Differences in CAPE range from 13% to over 30% relative to observations, demonstrating a model tendency to underestimate convective energy in highly unstable conditions. Tropopause height differences of 5–7% and modest freezing-level deviations also indicate sensitivity to upper-level dynamics.

Despite these discrepancies, the ECMWF model consistently reproduces the vertical temperature gradient, wind profile, and general thermodynamic pattern across multiple atmospheric layers. Therefore, while model outputs should be interpreted carefully when assessing convective intensity, the ECMWF remains a reliable tool for monitoring atmospheric stability and supporting

short-term weather prediction at Minangkabau International Airport and surrounding regions.

REFERENCES

[1] A. G. Kartasaputra, *Klimatologi: Pengaruh Iklim terhadap Tanah dan Tanaman*. Bumi Aksara, 1993. [Online]. Available: http://ucs.sulsellib.net//index.php?p=show_detail&id=49879

[2] R. M. White, "World climate conference: climate at the millennium," *Environment: Science and Policy for Sustainable Development*, vol. 21, no. 3, pp. 31–33, 1979.

[3] D. P. Djenal, F. Fatkhurrohman, and M. Putra, "Penerapan Internet of Things Sebagai Strategi Optimalisasi Pengamatan Udara Atas Menggunakan Ground Rasond Equipment," 2020. [Online]. Available: https://api.semanticscholar.org/CorpusID:230712591

[4] B. Alhadid, "Pemanfaatan Data Pengamatan Pilot Ballon untuk Analisis Kondisi Atmosfer sebelum Terjadinya Hujan Lebat di Wilayah Samarinda (Studi Kasus 2015 – 2022)," *Buletin GAW Bariri*, 2024, [Online]. Available: https://api.semanticscholar.org/CorpusID:270403762

[5] X. Wang and K. Wang, "Estimation of atmospheric mixing layer height from radiosonde data," *Atmos Meas Tech*, vol. 7, pp. 1701–1709, 2013, [Online]. Available: https://api.semanticscholar.org/CorpusID:54072420

[6] D. Derubertis, "Recent Trends in Four Common Stability Indices Derived from U.S. Radiosonde Observations," *J Clim*, vol. 19, pp. 309–323, 2006, [Online]. Available: https://api.semanticscholar.org/CorpusID:129264099

[7] M. D. Syaifullah, "Analisis Kondisi Udara Atas Wilayah Indonesia dengan Data Radiosonde," *Jurnal Meteorologi dan Geofisika*, vol. 18, no. 1, 2017.

[8] B. P. Syahputra, M. Yusuf, Y. D. Haryanto, and N. R. Florida, "Visualization of Aerological Diagram and Analysis of Atmospheric Sounding Information Using Raob with Model Data During Low Visibility Conditions at Cengkareng Meteorological Station," *Proceedings of International Conference on Multidiciplinary Research*, 2022, [Online]. Available: https://api.semanticscholar.org/CorpusID:254913329

A. Kristianto and A. P. Rani, "Kaitan Ketinggian Lapisan Batas Atmosfer Dengan Kondisi Cuaca Berdasrkan Profil Angin Vertikal Berbasis Pengamatan Radiosonde, Radar Cuaca, dan Keluaran Model WRF-ARW," *Jurnal Meteorologi Klimatologi dan Geofisika*, 2019, [Online]. Available: https://api.semanticscholar.org/CorpusID:197565240

] W. Qordowi, "Analisis Kondisi Atmosfer Terkait Kejadian Banjir Menggunakan Data Radiosonde dan Citra Satelit Himawari-8 (Studi Kasus : Sungai Liat, Kabupaten Bangka Tanggal 12 Februari 2018)," *Prosiding SNFA (Seminar Nasional Fisika dan Aplikasinya)*, 2019, [Online]. Available: https://api.semanticscholar.org/CorpusID:133803829

] WMO, "Significant Weather & Climate Event," 2023.

] M. G. Lawrence, "The relationship between relative humidity and the dewpoint temperature in moist air - A simple conversion and applications," *Bull Am Meteorol Soc*, vol. 86, pp. 225–233, 2005, [Online]. Available: https://api.semanticscholar.org/CorpusID:17152766

] O. A. Alduchov and R. E. Eskridge, "Improved Magnus form approximation of saturation vapor pressure," *Journal of Applied Meteorology (1988-2005)*, pp. 601–609, 1996.

] D. Camuffo, *Mixing Ratio—An overview of Science-Direct Topics*. 2019.

] WMO, *Guide to Instruments and Methods of Observation Volume IV-Space-based Observations*. 2021.

] P. Maccallini, "Absolute Humidity and Air Density," 2021.

] AMS, "Geopotential Height," 2024.

] I. T. Jolliffe and D. B. Stephenson, "FORECASTERS' FORUM Comments on 'Discussion of Verification Concepts in Forecast Verification: A Practitioner's Guide in Atmospheric Science,'" 2005. [Online]. Available: https://api.semanticscholar.org/CorpusID:52235155